catalysts

MDPI

Article

Au/TiO_2-CeO_2 Catalysts for Photocatalytic Water Splitting and VOCs Oxidation Reactions

Roberto Fiorenza [1], Marianna Bellardita [2], Luisa D'Urso [1], Giuseppe Compagnini [1], Leonardo Palmisano [2] and Salvatore Scirè [1,*]

[1] Dipartimento di Scienze Chimiche, Università di Catania, Viale A. Doria 6, 95125 Catania, Italy; rfiorenza@unict.it (R.F.); ldurso@unict.it (L.D.); gcompagnini@unict.it (G.C.)

[2] Dipartimento di Energia, Ingegneria dell'Informazione e modelli Matematici (DEIM), Università di Palermo, Viale delle Scienze 90128, Palermo, Italy; marianna.bellardita@unipa.it (M.B.); leonardo.palmisano@unipa.it (L.P.)

* Correspondence: sscire@unict.it; Tel.: +39-095-738-5112; Fax: +39-095-580-138

Academic Editor: Leonarda F. Liotta

Received: 1 July 2016; Accepted: 4 August 2016; Published: 10 August 2016

Abstract: Photocatalytic water splitting for H_2 production and photocatalytic oxidation of 2-propanol, an example of volatile organic compounds, were investigated over TiO_2 catalysts loaded with gold and/or ceria. In the water splitting reaction the presence of gold only slightly affected the performance of TiO_2 whereas the presence of CeO_2 had a more remarkable positive effect. In the 2-propanol oxidation Au/TiO_2 was the most active sample in terms of alcohol conversion whereas Au/TiO_2-CeO_2 exhibited the highest CO_2 yield. On the basis of characterization experiments (X-Ray Diffraction (XRD), Energy Dispersive X-ray Analysis EDX, surface area measurements, Diffuse Reflectance Spectroscopy (DRS) and Raman spectroscopy), it was suggested that the interaction of Au with TiO_2 causes an increase in the charge separation between the photo-excited electron/hole pairs, leading to an enhanced photocatalytic activity (to acetone over Au/TiO_2 and to CO_2 over Au/TiO_2-CeO_2), whereas the presence of ceria, acting as a hole trap, positively mainly affects the formation of hydrogen by water splitting.

Keywords: photocatalysis; gold; titanium dioxide; cerium oxide; H_2 production

1. Introduction

Since the publication of Fujishima and Honda [1], TiO_2 has extensively been used as a photocatalyst with growing interest both from an academic and industrial point of view. During this time, photocatalysis with TiO_2 was applied with various success to several reactions, among them H_2 production by water splitting or abatement of undesired and harmful organic compounds in air or water [2–8]. The good quantum yield and stability, high oxidative power, low cost and easy production [9–11] are the key reasons for the success of TiO_2.

By increasing the environmental concern, the removal of organic contaminants from air and water has become a key issue. Among eco-friendly methods of destroying recalcitrant organic pollutants, the advanced oxidation processes (AOPs) represent a valid alternative to conventional chemical methods. AOPs are based on in situ generation of reactive radical species, mainly $OH^{\bullet}$, by means of solar, chemical or other forms of energy [12,13]. In this field the photocatalytic oxidation (PCO) in the presence of TiO_2 to give total or partial oxidation of liquid or gaseous contaminants to benign substances is one of the most promising environmentally friendly techniques for the abatement of volatile organic compounds (VOCs) [14,15]. In fact, the formation of electron-hole pairs on TiO_2 by light irradiation with a suitable light source plays a key role in the mineralization of VOCs into CO_2 and H_2O.

Another important application of heterogeneous photocatalysis is the production of hydrogen by water splitting. Hydrogen, in fact, is regarded as an ideal fuel in sustainable clean energy production, being suitable for fuel cell technology. Unfortunately, at present, H_2 is mainly obtained from fossil fuels, such as natural gas, through the steam reforming process. Photochemical hydrogen generation via splitting of water by ultraviolet (UV) or visible light represents a total green alternative to its production.

TiO_2, however, presents some drawbacks: its wide band-gap energy (ca. 3.2 eV for anatase and 3.0 eV for rutile) makes it possible to use only about 5% of the solar spectrum and the high electron-hole recombination rate limits its photo-activity. In this regard, doping with metals or metal oxides could provide two positive effects: firstly, it could cause a decrease in the band gap energy, thus shifting the absorption band towards the visible region; secondly, the electron-hole recombination rate could be reduced by metal nanoparticles (NPs) acting as electron traps. In fact, several examples of titania doping with metals such as Fe [16,17], Pd [18], Pt [19,20], Cu [21] or other oxides as CeO_2 [22,23], ZnO [24,25] or SiO_2 [26] were reported in the literature.

Recently gold nanoparticles were used as an efficient doping system of TiO_2 [22,27–33]. Au-TiO_2 NPs showed, in fact, a strong absorption of the visible light due to the surface resonance plasmon (SPR) of their free electrons [27,28]. Therefore, the Au-TiO_2 plasmonic photocatalyst exhibited high efficiency in UV or visible light photo-activated reactions such as 2-propanol degradation [22,29], chemo-selective oxidation of alcohols [30], CO_2 reduction [31] and water splitting for H_2 and O_2 generation [32,33].

The enhancement of the performance under UV irradiation was ascribed to the more efficient interfacial charge transfer in the presence of metallic NPs whereas the emergence of high activity under visible irradiation was attributed to the occurrence of the SPR effect, which allows the absorption of visible light. To explain the above effects, two different roles of Au nanoparticles have been claimed in the literature: on the one hand, the photo-excited electrons of the gold surface plasmon can be injected into the TiO_2 conduction band, thus creating separated electron holes and then increasing their lifetime by hindering the recombination process [34]; on the other hand, Au NPs can favor electron transfer from the TiO_2 surface to the adsorbed molecular oxygen. The SPR phenomenon has been reported to be affected by the size, the shape, the content and the neighboring environment of gold NPs [29,35]. The above features of gold are particularly useful for photocatalytic water splitting; in fact, using excitation wavelengths matching the gold plasmon band, Au NPs absorb photons and inject electrons into the conduction band of the TiO_2. This latter effect is not common for a metal, but the nanometer size of Au particles and the occurrence of quantum size effects could be responsible for this mechanism and can explain the good activity of the Au/TiO_2 system for this reaction [32,33].

This work aims to evaluate how the presence of gold and/or ceria affects the chemico-physical properties and the photocatalytic activity of TiO_2 in the production of hydrogen by overall water splitting and in the oxidation of 2-propanol (chosen as the VOCs model).

2. Results and Discussion

2.1. H_2 Generation by Photocatalytic Water Splitting

The photo-activity of all investigated catalysts in the water splitting reaction ($H_2O \rightarrow H_2 + \frac{1}{2} O_2$), evaluated in terms of hydrogen evolution versus reaction time, is compared in Figure 1. For all samples, we observed the formation of O_2 in an almost stoichiometric amount (half moles than H_2), with only a slight defect of oxygen. By taking into account that the experiments were carried out in pure water without sacrificial agents, this confirms the occurrence of the water splitting reaction.

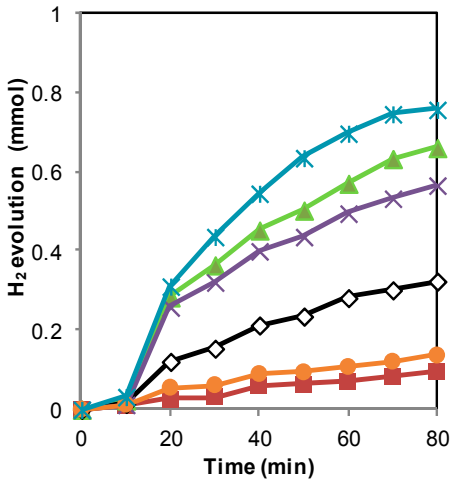

Figure 1. Photocatalytic H_2 production at 30 °C under ultraviolet (UV) irradiation over: TiO_2 (◇), CeO_2 (■), TiO_2-10%CeO_2 (▲), Au/TiO_2 (×), Au/CeO_2 (●) and Au/TiO_2-10%CeO_2 (✳).

For all samples it is possible to note that, after a short induction period (around 10 min), due to the stabilization of lamp irradiation and/or water saturation with evolved gases [36], hydrogen production firstly undergoes an almost linear increment for up to 40 min, followed by a moderate decrease of the production rate. According to the literature [37,38] this can be the result of two fundamental effects: (1) a recombination of charge carriers, namely the photo-generated electron-hole pairs, as electrons of the conduction band can quickly recombine with holes of the valence band, thus releasing energy as unproductive heat or photons; (2) a fast backward reaction, namely the recombination of hydrogen and oxygen into water. It is noteworthy that repetitive photocatalytic tests, using the same sample three times in succession, gave the same catalytic profile, with good data reproducibility, thus ruling out that hydrogen might partially arise from the presence of organic residues due to the synthesis, acting as sacrificial agents.

Interestingly, both bare TiO_2 (black line) and CeO_2 (brown line) samples showed some activity in the production of hydrogen which was found to increase in the presence of gold. The coupling of CeO_2 with TiO_2 positively affected the photocatalytic activity with a further increase obtained by the deposition of gold particles in the binary system of TiO_2-CeO_2. In fact, both TiO_2-10%CeO_2 (green line) and Au/TiO_2-10%CeO_2 (blue line) catalysts showed better performance than bare TiO_2 (H_2 evolution around two times higher) and Au/TiO_2 (H_2 evolution around 25% higher). As reported in the literature, despite the bulk ceria and titania not having a similar crystal structure, cerium ions (Ce^{3+} and Ce^{4+}) can replace the Ti^{4+} ions, modifying the physicochemical properties of TiO_2. Such an interaction between the CeO_2 and TiO_2 frameworks could be the key factor explaining the enhancement of the photocatalytic activity of this mixed oxide system towards water splitting [39,40]. The metal atoms, instead, pile up the electrons from the TiO_2 conduction band and transfer them to hydrogen protons, acting as H_2 evolution centers.

2.2. Photocatalytic Oxidation of 2-Propanol

Figure 2 shows the activity data at 25 °C of the 2-propanol photocatalytic oxidation on all tested catalysts in terms of alcohol conversion (Figure 2a), selectivity to acetone (Figure 2b), selectivity to CO_2 (Figure 2c), and yield to CO_2 (Figure 2d). It must be noted that the first point was taken after 20 min to allow the lamp to reach a stable energy status.

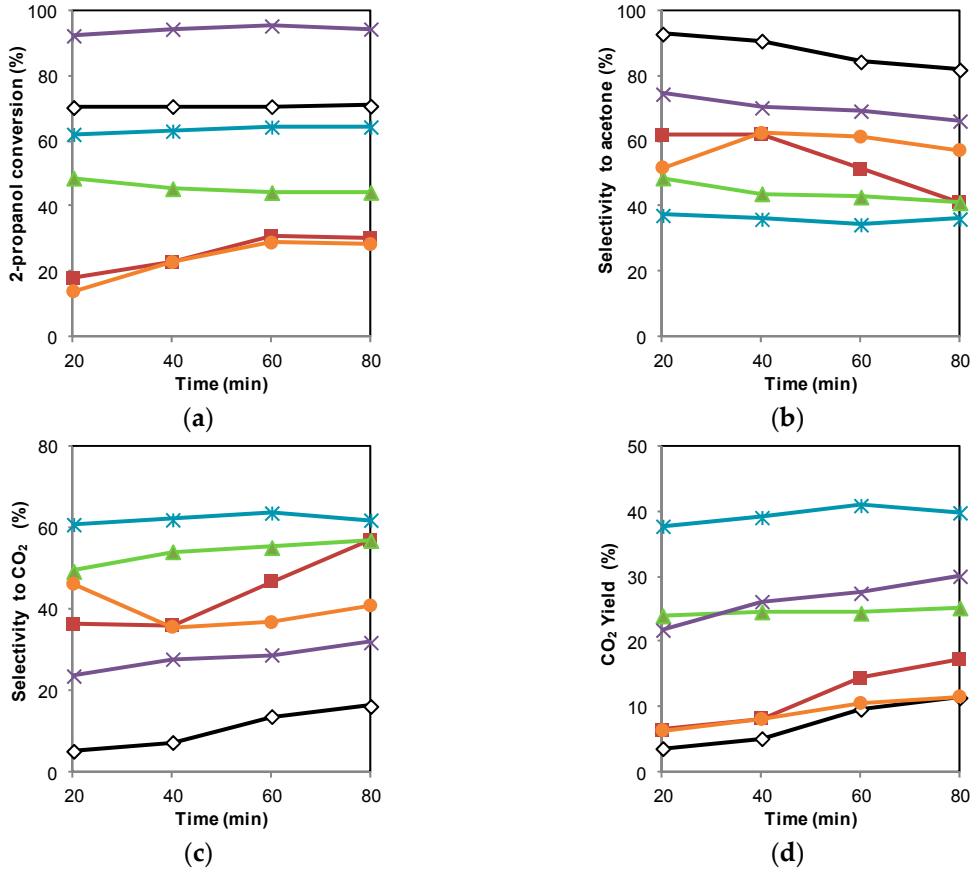

Figure 2. Photocatalytic 2-propanol oxidation over: TiO_2 (◇), CeO_2 (■), TiO_2-10%CeO_2 (▲), Au/TiO_2 (×), Au/CeO_2 (●) and Au/TiO_2-10%CeO_2 (✳): (**a**) 2-propanol conversion; (**b**) Selectivity to acetone; (**c**) Selectivity to CO_2; (**d**) Yield to CO_2.

The partial oxidation of 2-propanol can proceed with two reaction pathways [41,42]: the oxidative dehydrogenation to acetone and water or the dehydration to propene. Over Au/CeO_2 and CeO_2 catalysts no propene was formed during the photocatalytic tests, whereas over TiO_2-based samples (TiO_2, TiO_2-10%CeO_2, Au/TiO_2 and Au/TiO_2-10%CeO_2) the formation of propene occurred to a very low extent (1%–3% selectivity). In this latter case, the formation of propene can be ascribed to the more acidic character of TiO_2 with respect to CeO_2 [43,44].

Considering the conversion of 2-propanol (Figure 2a), the best results were found over the Au/TiO_2 catalyst (violet line), which was more active than, in order, TiO_2 (black line), Au/TiO_2-10%CeO_2 (blue line) and TiO_2-10%CeO_2 samples (green line). The increase of TiO_2 photocatalytic activity in the presence of Au particles can be ascribed to the different Fermi levels of the two species leading to an increased charge separation between the excited electron (e^-) and the hole (h^+) [45–47]. The high activity of the Degussa P25 TiO_2 used in this work can be due to the occurrence of an interaction between the two phases of TiO_2 (80% anatase, 20% rutile) that increases both the charge carrier (electron-hole) separation and the total photo-efficiency [48,49]. The bare CeO_2 (dark red curve) and the Au/CeO_2 (orange curve) samples exhibited a low activity for the conversion of 2-propanol (maximum conversion of around 30%), while the presence of ceria negatively affected the performance of TiO_2, the maximum conversion being, in fact, lower on TiO_2-10%CeO_2 (50%) compared to TiO_2 (70%). Differently from TiO_2, the presence of gold did not affect the CeO_2 performances, with the 2-propanol conversion being almost the same for CeO_2 and Au/CeO_2 samples.

The selectivity to acetone (Figure 2b) generally showed a slight decrease over time, with a corresponding increase in the selectivity to CO_2. The bare TiO_2 displayed the highest selectivity

according to data reported in the literature for this reaction [18,49], whereas the presence of CeO_2 or Au had a negative effect on the acetone selectivity, causing a decrease of the maximum value from 95% over TiO_2 to 70% over Au/TiO_2, 50% over TiO_2-10%CeO_2 and 40% over Au/TiO_2-10%CeO_2. Consequently, the selectivity for CO_2 (Figure 2c) and the yield of CO_2 (Figure 2d), defined as the product of the 2-propanol conversion and the CO_2 selectivity, had a reverse trend, with the Au/TiO_2-10%CeO_2 system exhibiting the highest values of CO_2 selectivity. These results suggest that the presence of gold and/or CeO_2 improved the total oxidation of 2-propanol to CO_2 more than its selective oxidation to acetone.

2.3. Discussion

The catalytic activity data reported in the preceding section clearly pointed out that gold and/or CeO_2 affected the photocatalytic performance of TiO_2 differently, depending on the reaction taken into consideration.

In particular, in the photocatalytic water splitting (Figure 1), the presence of gold produced an increase of the hydrogen production both on TiO_2 and on CeO_2. The rate of H_2 production was further enhanced by using ternary Au/TiO_2-CeO_2 systems, the co-presence of gold and ceria leading to the highest hydrogen evolution.

Also in the photocatalytic 2-propanol oxidation (Figure 2), the presence of gold was necessary to obtain a good performance, with Au/TiO_2 being the most active sample for the alcohol conversion and Au/TiO_2-10%CeO_2 being the catalyst showing the best mineralization yield. The effect of CeO_2 addition to TiO_2 was instead detrimental for the 2-propanol conversion, resulting, however, in a considerable increase in the CO_2 yield.

The chemico-physical characterization of the investigated Au/TiO_2-CeO_2 catalysts helped us to rationalize the above results. The main properties of the catalysts are displayed in Table 1. As revealed by XRD measurements, and reported by some of us in a previous paper [22], TiO_2 anatase was the main crystal phase for all samples, and the presence of CeO_2 and/or Au caused a slight decrease in the crystallites' size. The Raman spectra (Figure 3a), exhibiting bands at around 150 cm^{-1}, 403 cm^{-1}, 524 cm^{-1} and 647 cm^{-1}, confirmed that anatase was the main TiO_2 polymorphic phase in these samples [50,51]. The Au/TiO_2 sample (red line) showed the same bands of bare TiO_2 (black line). In the TiO_2-10%CeO_2 sample (green line) the signal at 466 cm^{-1} was associated with the cubic phase of the CeO_2 fluorite [52–54] and the small component at 600 cm^{-1} was assignable to intrinsic O vacancies in ceria as a result of its non-stoichiometric composition due to the presence of Ce^{3+} in the lattice [54,55].

Table 1. Chemico-physical properties of Au/TiO_2-CeO_2 catalysts.

Sample	Surface Area (m^2/g)	E_g (eV)	Crystallite Size (nm) [a]	Crystal Phase [a]
TiO_2	44.8	2.98	24	TiO_2 Anatase-Rutile
CeO_2	110.2	2.90	10	CeO_2 Fluorite
TiO_2-10%CeO_2	47.5	2.93	22	TiO_2 Anatase-Rutile CeO_2 Fluorite
Au/TiO_2	46.4	2.97	21	TiO_2 Anatase-Rutile
Au/CeO_2	112.7	2.95	11	CeO_2 Fluorite
Au/TiO_2-10%CeO_2	50.5	2.96	19	TiO_2 Anatase-Rutile, CeO_2 Fluorite

[a] Estimated by XRD measurements.

Interestingly, over the Au/TiO_2-10%CeO_2 sample, the peak associated with cubic CeO_2 was less intense, broader and shifted to lower frequencies compared to over the TiO_2-10%CeO_2 sample (Figure 3b, orange and green lines, respectively). This could be due to a less crystalline and more

defective structure of ceria in the presence of gold. In fact, Raman has been reported to be sensitive to the degree of crystallinity of samples, with broader, less intense Raman peaks in the case of less crystalline material [56].

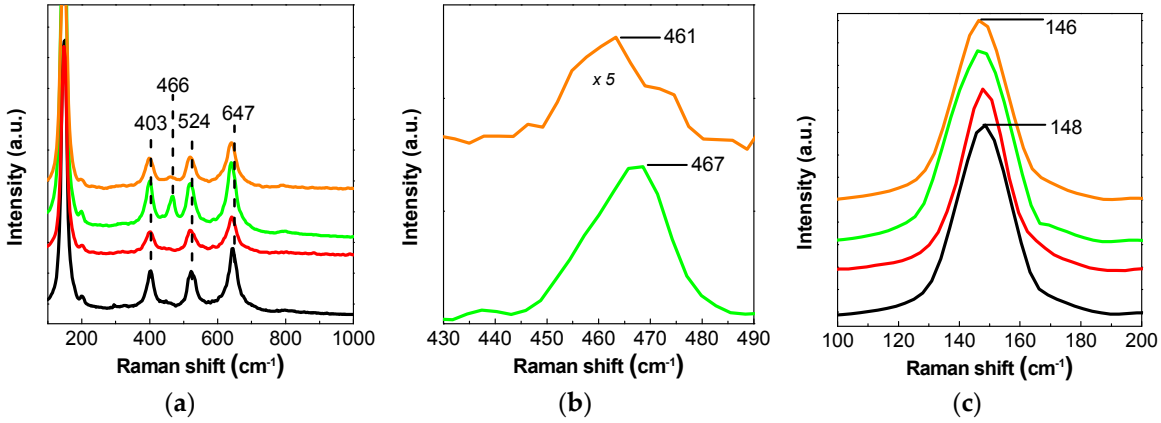

Figure 3. (**a**) Vibrational modes of Raman spectra of TiO_2 (—), Au/TiO_2 (—), TiO_2-10%CeO_2 (—), and Au/TiO_2-10%CeO_2 (—) samples; (**b**) Raman shift of the signal of cubic CeO_2 in TiO_2-10%CeO_2 (—), and Au/TiO_2-10%CeO_2 (—) samples; (**c**) Raman shift of the main E_g vibrational mode of TiO_2 anatase in TiO_2 (—), Au/TiO_2 (—), TiO_2-10%CeO_2 (—), and Au/TiO_2-10%CeO_2 (—) samples.

Figure 3c shows the position of the main vibrational mode of anatase E_g, pointing out that there was only a slight red shift (about 2 cm^{-1}) on the TiO_2-10%CeO_2 and Au/TiO_2-10%CeO_2 samples. By considering that the E_g anatase mode at 148 cm^{-1} is associated with the O-Ti-O vibration, the presence of CeO_2 in the TiO_2 lattice could probably cause a bond distortion resulting in the observed shift of the vibration band.

To analyze the distribution of cerium oxide on TiO_2 a Raman mapping analysis was performed. This technique allows non-destructive and non-invasive analysis of features such as the separation of chemical species in multi-component samples. Chemical maps of TiO_2 and CeO_2 nanostructures performed on the TiO_2-10%CeO_2 sample, based on the detailed Raman image (over a 15 µm × 15 µm image scan, with 150 points per line and 150 lines per image), are presented in Figure 4.

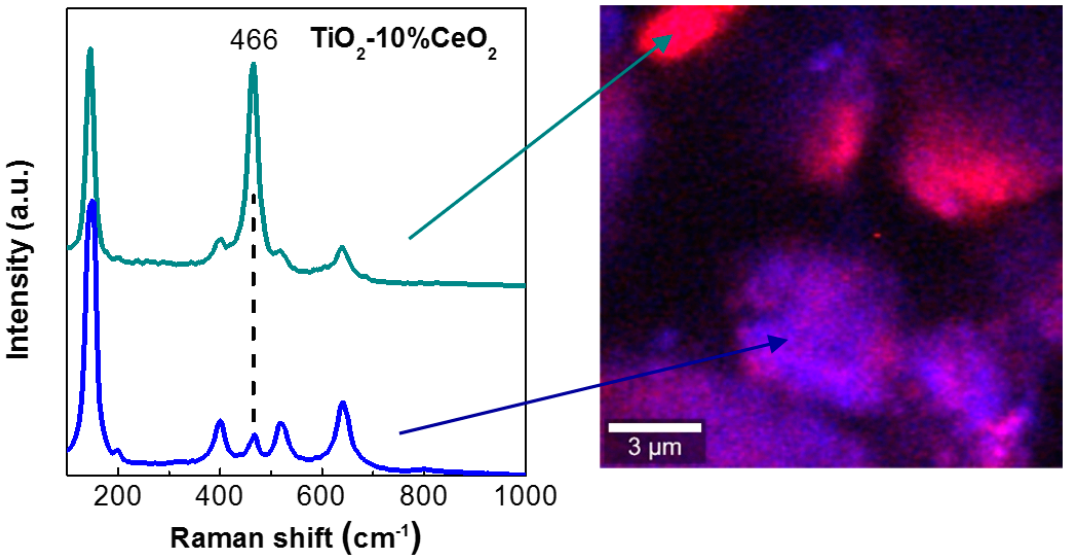

Figure 4. Confocal Raman mapping image of TiO_2-10%CeO_2 sample.

Representative spectra of two different regions are reported in red and violet color scales. The spectra show almost identical features but with very different intensities. The CeO_2 characteristic band (466 cm^{-1}) of higher intensity was recorded in the red region, while in the violet region TiO_2 peaks (150 cm^{-1}, 403 cm^{-1}, 524 cm^{-1} and 647 cm^{-1}) are very visible with the ceria band of decreased intensity (according to the 10%), pointing out that the ceria was not homogenously dispersed on the TiO_2 bulk.

The band-gap energy values (Table 1), estimated by reporting the modified Kubelka-Munk function, $[F(R_\infty')h\nu]^{1/2}$ against the exciting light energy [57], showed that the TiO_2-10%CeO_2 sample had a lower E_g (2.93 eV) compared to the bare TiO_2 (2.98 eV). This can be related to the replacement of Ti^{4+} cations by Ce^{4+} or Ce^{3+} cations in the TiO_2 network [51,54,58]. Moreover, looking at the DRS spectra of the investigated samples in the visible region (Figure 5), it can be seen that all gold-loaded samples (Au/TiO_2, Au/CeO_2 and Au/TiO_2-10%CeO_2) exhibit a clear absorbance band at around 550 nm, attributed to the plasmon resonance of gold nanoparticles [59]. As reported in the literature, the photo-excited electrons of the gold surface plasmon can be injected to the TiO_2 conduction band, thus creating separated electrons and holes and then increasing their lifetime by hindering the recombination process [29,32–35]. It must be underlined that no significant variation in the surface area (Brunauer-Emmett-Teller (BET) analysis) of investigated samples was detected in the presence of gold and/or CeO_2. It must also be noted that the bare TiO_2 showed a surface area of 44.8 m^2g^{-1}, lower than the values found in the literature for P25 TiO_2 (50−54 m^2g^{-1}), reasonably due to the thermal pretreatment of TiO_2 (calcination at 350 °C) [60].

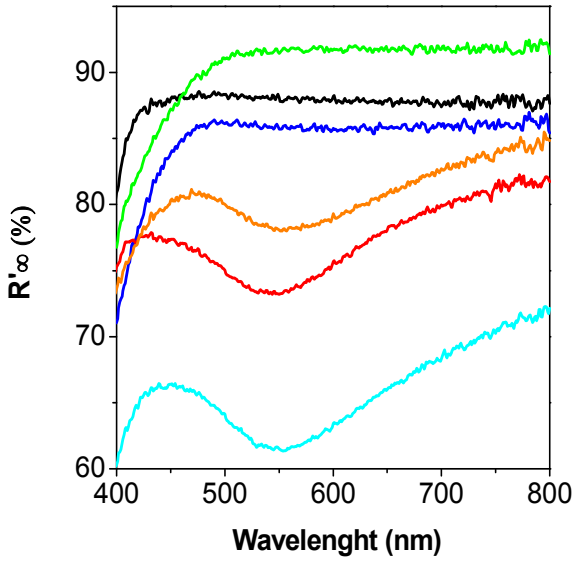

Figure 5. Diffuse Reflectance Spectroscopy (DRS) spectra (visible region) of CeO_2 (—) TiO_2 (—), TiO_2-10%CeO_2 (—), Au/TiO_2 (—), Au/CeO_2 (—) and Au/TiO_2-10%CeO_2 (—) samples.

The surface EDX analysis of investigated samples is reported in Figure 6. It is possible to note that the signals related to cerium (at 4.8 and 5.3 KeV, the first one overlapped with the signal of Ti) were more intense for the Au/TiO_2-10%CeO_2 system. Moreover, the elemental composition of these catalysts showed that on Au/TiO_2-10%CeO_2, the Ce atomic percentage is about four times greater than that found on TiO_2-10%CeO_2 (5.1% and 1.2%, respectively), indicating that the presence of gold on TiO_2-CeO_2 oxide leads to a remarkable cerium surface enrichment.

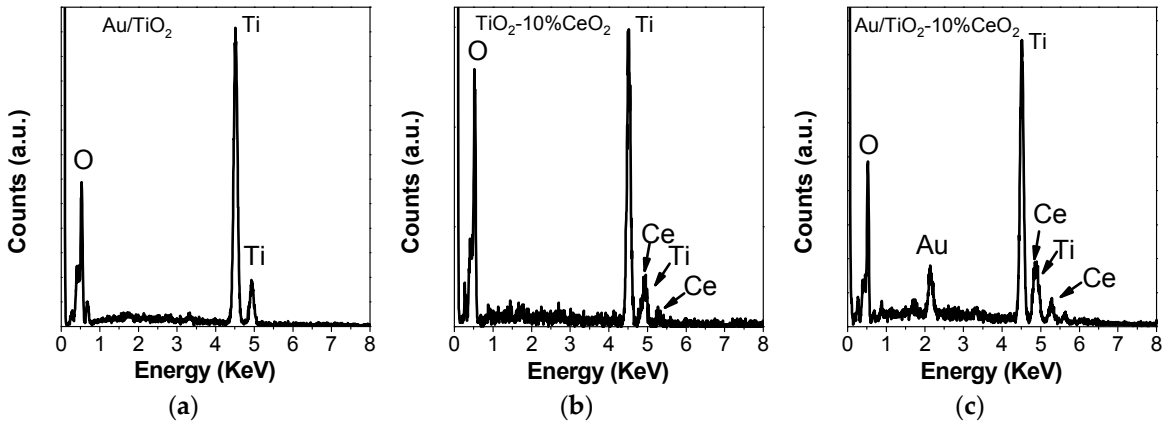

Figure 6. EDX (Energy-dispersive X-ray spectroscopy) spectra of (**a**) Au/TiO_2, (**b**) TiO_2-10%CeO_2 and (**c**) Au/TiO_2-10%CeO_2 samples.

The different role of gold and CeO_2 in affecting the properties and the catalytic behavior of TiO_2 in the photo-oxidation and the photoreduction reactions investigated here could be rationalized by taking into account the surface active species involved in these reactions. As for the photocatalytic water/air oxidative purification, the photocatalytic hydrogen production essentially requires photo-generation of hole/electron pairs. Nevertheless, the role of holes/electrons, as well as the surface reactions involved, are different. In fact, in the photocatalytic oxidation, valence band (VB) holes are the key elements involved in the removal of contaminants, whereas in H_2 production via photocatalytic water splitting reducing Conduction Band (CB) electrons becomes crucial as their role is mainly that of reducing protons to hydrogen molecules.

The addition of gold to TiO_2 results in an enhancement of the photocatalytic activity towards 2-propanol oxidation, due to an increase in the charge separation between the excited electron and the hole of the titania [45,46,61]. The proposed scheme of the electron transfer phenomena taking place in the Au/TiO_2-CeO_2 system is illustrated in Figure 7. We must underline that under the irradiation conditions used in this work (medium pressure Hg lamp, providing UV and to a lesser extent visible photons), the SPR effect of Au nanoparticles, involving an inverse transfer of electrons from Au to the CB of TiO_2, should play a minor role, becoming important only when visible light is used as the irradiation source. Interestingly, when the cerium oxide was also present, photo-generated active species (superoxide oxygen and hydroxyl radicals) could allow an easier re-oxidation of ceria, thus speeding up its redox process [22,23]. These processes were beneficial for the complete oxidation to CO_2. Furthermore, the basic and redox characteristics of CeO_2 sites with respect to the more acid TiO_2 sites could facilitate the direct combustion of 2-propanol to CO_2 [42,62], resulting in the highest CO_2 yield over the Au/TiO_2-10%CeO_2 system.

The surface mechanisms induced by gold were less efficient for the photocatalytic water splitting. In fact, even if the photo-generated electrons and holes have potentials which are thermodynamically adequate for the water splitting, they tend to recombine with each other if the number of surface active sites for the redox reaction is not sufficient. In this case, the substitution of cerium ions (Ce^{3+} and Ce^{4+}) in the TiO_2 framework, as suggested by DRS measurements, was the key factor for having a good performance. The cerium defects act, in fact, as hole traps [39,40,63], avoiding the recombination of active electrons and holes and thus favoring the reduction of water. In this case, gold positively affects the photocatalytic performance, both increasing the defective structure of ceria, as shown by Raman, and favoring the enrichment of ceria on the surface of TiO_2, as shown by EDX, thus explaining the highest H_2 production rate of the Au/TiO_2-10%CeO_2 system.

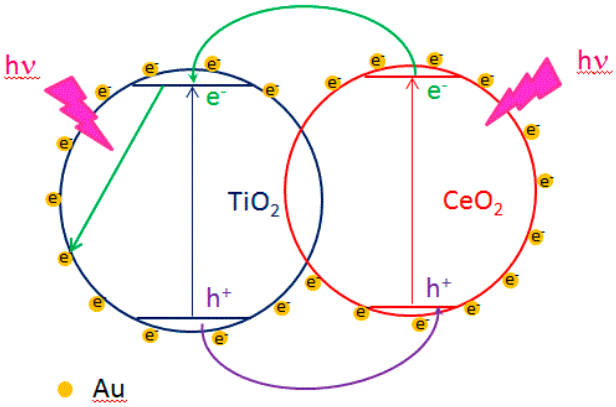

Figure 7. Scheme of the electron transfer phenomena taking place in the Au/TiO_2-CeO_2 system by irradiation with UV light.

3. Materials and Methods

3.1. Catalyst Preparation

TiO_2 used in this work was commercial P25 Degussa (Degussa, Frankfurt, Germany). CeO_2 was instead prepared by precipitation with KOH 0.1 M (Fluka, Buchs, Switzerland) from $Ce(NO_3)_3 \cdot 6H_2O$ (Fluka, Buchs, Switzerland) water solution, filtration and treatment in air at 450 °C for 4 h of the obtained powder. Mixed TiO_2-CeO_2 composites were prepared with 10 wt. percent of CeO_2, according to the following procedure: aliquots of TiO_2 were impregnated with an appropriate amount of $Ce(NO_3)_3 \cdot 6H_2O$ solution, the obtained slurries were stirred for 4 h, dried at 120 °C and finally treated in air at 350 °C for 4 h. Calcination in air at 350 °C for 4 h was also carried out on the bare TiO_2.

Gold (1 wt %) was loaded on the bare or mixed TiO_2-CeO_2 oxides by deposition-precipitation. After the pH of the aqueous solution of the Au precursor ($HAuCl_4$, Sigma-Aldrich, Buchs, Switzerland) was adjusted to the value of 8 by 0.1 M aqueous solution of KOH, the support was added under stirring (500 rpm), keeping the slurry at 70 °C for 3 h, then digesting for 24 h, filtering and washing several times (until chlorides disappearance), drying at 110 °C and finally grounding before use.

3.2. Catalyst Characterization Experiments

X-ray diffraction (XRD) was performed with a Bruker AXSD5005 XRD (Bruker, Karlsruhe, Germany) instrument using Cu Kα radiation. Peaks of crystalline phases were compared with those of standard compounds of the JCPDS Data File (Bruker, Diffrac. Suite™ Software package Karlsruhe, Germany).

Energy-dispersive X-ray spectroscopy (EDX) was carried with an INCA Energy Oxford solid state detector (Oxford Instruments plc, Tubney Woods, Abingdon, Oxfordshire, United Kingdom). A field emission gun scanning electron microscopy (FE-SEM, (Carl Zeiss SMT AG Company, Oberkochen, Germany) equipped with a ZEISS SUPRA 55 VP microscope was used to determine the morphologies of the investigated samples.

Raman spectra were recorded with a WITec alpha 300 confocal Raman system (WITec Wissenschaftliche Instrumente und Technologie GmbH Ulm, Germany). The excitation source for Raman measurement was a 532 nm laser line of a Coherent Compass Sapphire Laser. All measurements were performed at low irradiation power to avoid laser induced heating. A 100× objective lens with a NA = 0.90 was used.

UV-VIS reflectance spectra were performed by diffuse reflectance spectroscopy (DRS, with a Shimadzu UV-2401 PC instrument (Shimadzu Corporation, Kyoto, Japan), recording spectra in the range 200–800 nm and using $BaSO_4$ as reference sample.

Surface area measurements were carried out with a Sorptomatic series 1990 (Thermo Quest, Milano, Italy) instrument using the BET nitrogen adsorption method. All samples were previously outgassed (10^{-3} Torr) at 120 °C.

3.3. Photocatalytic Activity Experiments

The 2-propanol photo-oxidation was performed in a home-made Pyrex cylindrical shape photo-reactor) (diameter 58 mm, height 100 mm) at 25 °C and atmospheric pressure in gas–solid regime. Then 300 mg of catalyst were placed inside the reactor with a porous inlet glass septum allowing homogeneous distribution of the inlet gas mixture. This mixture consisted of 2-propanol (0.1 mM) and air (flow rate of 20 cm^3min^{-1}). An UV Helios-Italquartz 125 W medium pressure Hg lamp (Helios Italquartz Srl, Milano, Italy) was used as the irradiation source. Water flowed through a jacket surrounding the lamp to cut-off the infrared radiation and to maintain constant the temperature inside the reactor. The lamp radiant power in the range 300−400 nm, measured by a radiometer Delta Ohm DO9721 (Delta Ohm Srl, Padova, Italy), was equal to 1.5 mW cm^{-2}. The evolution of the species formed during the runs was followed by withdrawing 500 μl of gas from the reactor by a gas-tight syringe. The 2-propanol and acetone were detected by a Shimadzu GC 2010 (Shimadzu Corporation, Kyoto, Japan) equipped with a Phenomenex Zebron Wax-Plus (30 μm × 0.32 μm × 0.53 μm) column and a FID detector while CO_2 was measured by a HP 6890 Series GC (Agilent Technologies, Santa Clara, CA, US) System equipped with a Supelco packed column GC 60/80 Carboxen™-1000 and a thermal conductivity detector using Helium as carrier gas. The carbon balance was always higher than 95%.

Hydrogen generation by photocatalytic water splitting was performed in a home-made Pyrex jacketed reactor thermostated at 30 °C. The reactor headspace was linked to an inverted buret, filled with water at atmospheric pressure. This allows the quantification of the evolved gas. The evolution of H_2 was confirmed by analyzing the effluent gases with an online gas chromatograph (HP 6890 Series GC System, Agilent Technologies, Santa Clara, CA, US) equipped with a packed column (Carboxen 1000) and thermal conductivity detector. Specifically, the catalyst (50 mg) was placed inside the photo-reactor, with 100 mL of deionized water under stirring. The suspension was purged with a nitrogen flow for at least 30 min before irradiation in order to remove dissolved air. The suspension was then irradiated for 80 minutes using a 100 W mercury lamp.

4. Conclusions

The photocatalytic performance of the Au/TiO_2-CeO_2 system was studied both in the oxidation of 2-propanol and in the water splitting reaction. Characterization experiments (XRD, EDX, surface area measurements, DRS and Raman spectroscopy) allowed us to suggest that the interaction of gold with TiO_2 causes an increase in the photocatalytic oxidation activity, due to a charge separation enhancement between the excited electron and the hole of TiO_2. The co-existence of Au and both TiO_2 and CeO_2 oxides favors the mineralization of the alcohol. In the water splitting reaction, the presence of ceria, acting as a hole trap, is essential to have a high hydrogen production rate, while Au conveys the electron transfer from TiO_2 to the H^+ ions. Notably, the SPR effect of Au nanoparticles could induce electron transfer to the CB of TiO_2, but the SPR, described as relevant when visible light is used, would play a minor role in our case (both UV and visible light irradiation).

Acknowledgments: Authors would like to acknowledge the Bio-nanotech Research and Innovation Tower (BRIT) project that supports this research activity.

Author Contributions: R.F. and M.B. conceived and performed the photocatalytic experiments and XRD, EDX, DRS and BET characterization, L.D. e G.C. performed and discussed Raman analysis, S.S. and L.P. conceived the idea of writing the paper, supervised the work and edited the article.

Conflicts of Interest: The authors declare no conflict of interest.

References

1. Fujishima, A.; Honda, K. Electrochemical Photolysis of Water at a Semiconductor Electrode. *Nature* **1972**, *238*, 37–38. [CrossRef] [PubMed]
2. Liao, C.H.; Huang, C.W.; Wu, J.C.S. Hydrogen Production from Semiconductor-based Photocatalysis via Water Splitting. *Catalysts* **2012**, *2*, 490–516. [CrossRef]
3. Zou, Z.; Ye, J.; Sayama, K.; Arakawa, H. Direct splitting of water under visible light irradiation with an oxide semiconductor photocatalyst. *Nature* **2001**, *414*, 625–627. [CrossRef] [PubMed]
4. Herrmann, J.M. Heterogeneous photocatalysis: Fundamentals and applications to the removal of various types of aqueous pollutants. *Catal. Today* **1999**, *53*, 115–129. [CrossRef]
5. Ibhadon, A.O.; Fitzpatrick, P. Heterogeneous Photocatalysis: Recent Advances and Applications. *Catalysts* **2013**, *3*, 189–218. [CrossRef]
6. Chen, X.; Mao, S.S. Titanium Dioxide Nanomaterials: Synthesis, Properties, Modifications and Applications. *Chem. Rev.* **2007**, *107*, 2891–2959. [CrossRef] [PubMed]
7. Lazar, M.A.; Varghese, S.; Nair, S.S. Photocatalytic Water Treatment by Titanium Dioxide: Recent Updates. *Catalysts* **2012**, *2*, 572–601. [CrossRef]
8. Gaya, U.I.; Abdullah, A.H. Heterogeneous photocatalytic degradation of organic contaminants over titanium dioxide: A review of fundamentals, progress and problems. *J. Photochem. Photobiol. C* **2008**, *9*, 1–12. [CrossRef]
9. Hisanga, T.; Harada, K.; Tanaka, K. Photocatalytic degradation of organochlorine compounds in suspended TiO_2. *J. Photochem. Photobiol. A* **1990**, *54*, 113–118. [CrossRef]
10. Wang, C.; Ying, J. Sol-Gel Synthesis and Hydrothermal Processing of Anatase and Rutile Titania Nanocrystals. *Chem. Mater.* **1999**, *11*, 3113–3120. [CrossRef]
11. Pillai, S.C.; Periyat, P.; George, R.; McCormack, D.E.; Seery, M.K.; Hayden, H.; Colreavy, J.; Corr, D.; Hinder, S.J. Synthesis of high-temperature stable anatase TiO_2 photocatalyst. *J. Phys. Chem. C* **2007**, *111*, 1605–1611. [CrossRef]
12. Kudo, T.; Nakamura, Y.; Ruike, A. Development of rectangular column structured titanium oxide photocatalysts anchored on silica sheets by a wet process. *Res. Chem. Intermed.* **2003**, *29*, 631–639. [CrossRef]
13. Bahnemann, D. Photocatalytic water treatment: Solar energy applications. *Sol. Energy* **2004**, *77*, 445–459. [CrossRef]
14. Zeltner, W.A.; Tompkin, D.T. Shedding Light on Photocatalysis. In *ASHRAE Transactions, Part 2*; ASHRAE: Atlanta, GA, USA, 2005; Volume 111, pp. 523–532.
15. Einaga, H.; Mochiduki, K.; Teraoka, Y. Photocatalytic Oxidation Processes for Toluene Oxidation over TiO_2 Catalysts. *Catalysts* **2013**, *3*, 219–231. [CrossRef]
16. Zhao, B.; Mele, G.; Pio, I.; Li, J.; Palmisano, L.; Vasapollo, G. Degradation of 4-nitrophenol (4-NP) using Fe-TiO_2 as a heterogeneous photo-Fenton catalyst. *J. Haz. Mat.* **2010**, *176*, 569–574. [CrossRef] [PubMed]
17. Arana, J.; Dona-Rodriguez, J.M.; Gonzalez-Diaz, O.; Tello Rendon, E.; Herrera Melian, J.A.; Colon, G.; Navìo, J.A.; Perez Pena, J. Gas-phase ethanol photocatalytic degradation study with TiO_2 doped with Fe, Pd and Cu. *J. Mol. Catal. A* **2004**, *215*, 153–160. [CrossRef]
18. Colmenares, J.C.; Aramendia, M.A.; Marinas, A.; Marinas, J.M.; Urbano, F.J. Synthesis, characterization and photocatalytic activity of different metal-doped titania systems. *Appl. Catal. A: Gen.* **2006**, *306*, 120–127. [CrossRef]
19. Bashir, S.; Wahab, A.K.; Idriss, H. Synergism and photocatalytic water splitting to hydrogen over M/TiO_2 catalysts: Effect of initial particle size of TiO_2. *Catal. Today* **2015**, *240*, 242–247. [CrossRef]
20. Bellardita, M.; García-López, E.I.; Marcì, G.; Palmisano, L. Photocatalytic formation of H_2 and value-added chemicals in aqueous glucose (Pt)-TiO_2 suspension. *Int. J. Hydrog. Energy* **2016**, *41*, 5934–5947. [CrossRef]
21. Gombac, V.; Sordelli, L.; Montini, T.; Delgado, J.J.; Adamski, A.; Adami, G.; Cargnello, M.; Bernal, S.; Fornasiero, P. CuO_x-TiO_2 Photocatalysts for H_2 Production from Ethanol and Glycerol Solutions. *J. Phys. Chem. A* **2010**, *114*, 3916–3925. [CrossRef] [PubMed]
22. Fiorenza, R.; Bellardita, M.; Palmisano, L.; Sciré, S. A comparison between Photocatalytic and Catalytic oxidation of 2-Propanol over Au/TiO_2-CeO_2 catalysts. *J. Mol. Catal. A: Chem.* **2016**, *415*, 56–64. [CrossRef]

23. Zeng, M.; Li, Y.; Mao, M.; Bai, J.; Ren, L.; Zhao, X. Synergetic Effect between Photocatalysis on TiO_2 and Thermocatalysis on CeO_2 for Gas-Phase Oxidation of Benzene on TiO_2/CeO_2 Nanocomposites. *ACS Catal.* **2015**, *5*, 3278–3286. [CrossRef]
24. Marcì, G.; Augugliaro, V.; Lopez-Munoz, M.J.; Martın, C.; Palmisano, L.; Rives, V.; Schiavello, M.; Tilley, R.J.D.; Venezia, A.M. Preparation Characterization and Photocatalytic Activity of Polycrystalline ZnO/TiO_2. *J. Phys. Chem. B* **2001**, *105*, 1026–1032.
25. Pérez-Larios, A.; Lopez, R.; Hernández-Gordillo, A.; Tzompantzi, F.; Gómez, R.; Torres-Guerra, L.M. Improved hydrogen production from water splitting using TiO_2-ZnO mixed oxides. *Fuel* **2012**, *100*, 139–143. [CrossRef]
26. Bellardita, M.; Addamo, M.; Di Paola, A.; Marcì, G.; Palmisano, L.; Cassar, L.; Borsa, M. Photocatalytic activity of TiO_2/SiO_2 systems. *J. Haz. Mat.* **2010**, *174*, 707–713. [CrossRef] [PubMed]
27. Wang, P.; Huang, B.; Dai, Y.; Whangbo, M.H. Plasmonic photocatalysts: Harvesting visible light with noble metal nanoparticles. *Phys. Chem. Chem. Phys.* **2012**, *149*, 9813–9825. [CrossRef] [PubMed]
28. Orendorff, C.J.; Sau, T.K.; Murphy, C.J. Shape-Dependent Plasmon-Resonant Gold Nanoparticles. *Small* **2006**, *2*, 636–639. [CrossRef] [PubMed]
29. Kowalska, E.; Mahaney, O.O.P.; Abe, R.; Ohtani, B. Visible-light-induced photocatalysis through surface plasmon excitation of gold on titania surfaces. *Phys. Chem. Chem. Phys.* **2010**, *12*, 2344–2355. [CrossRef] [PubMed]
30. Naya, S.I.; Inoue, A.; Tada, H. Self-Assembled Heterosupramolecular Visible Light Photocatalyst Consisting of Gold Nanoparticle-Loaded Titanium(IV) Dioxide and Surfactant. *J. Am. Chem. Soc.* **2010**, *132*, 6292–6293. [CrossRef] [PubMed]
31. Hou, W.; Hung, W.H.; Pavaskar, P.; Goeppert, A.; Aykol, M.; Cronin, S.B. Photocatalytic conversion of CO_2 to hydrocarbon fuels via plasmon-enhanced absorption and metallic interband transitions. *ACS Catal.* **2011**, *1*, 929–936. [CrossRef]
32. Jovic, V.; Chen, W.T.; Sun-Waterhouse, D.; Blackford, M.G.; Idriss, H.; Waterhouse, G.I.N. Effect of gold loading and TiO_2 support composition on the activity of Au/TiO_2 photocatalysts for H_2 production from ethanol-water mixtures. *J. Catal.* **2013**, *305*, 307–317. [CrossRef]
33. Hinojosa-Reyes, M.; Hernández-Gordillo, A.; Zanella, R.; Rodríguez-González, V. Renewable hydrogen harvest process by hydrazine as scavenging electron donor using gold TiO_2 photocatalysts. *Catal. Today* **2016**, *266*, 2–8. [CrossRef]
34. Silva, C.G.; Juarez, R.; Tiziana, M.; Molinari, R.; Garcia, H. Influence of Excitation Wavelength (UV or Visible Light) on the Photocatalytic Activity of Titania Containing Gold Nanoparticles for the Generation of Hydrogen or Oxygen from Water. *J. Am. Chem. Soc.* **2011**, *133*, 595–602. [CrossRef] [PubMed]
35. Zhang, J.Z.; Noguez, C. Plasmonic Optical Properties and Applications of Metal Nanostructures. *Plasmonics* **2008**, *3*, 127–150. [CrossRef]
36. Galińska, A.; Walendziewski, J. Photocatalytic Water Splitting over Pt−TiO_2 in the Presence of Sacrificial Reagents. *Energy Fuels* **2005**, *19*, 1143–1147. [CrossRef]
37. Ni, M.; Leung, M.K.H.; Leung, D.Y.C.; Sumathy, K. A review and recent developments in photocatalytic water-splitting using TiO_2 for hydrogen production. *Renew. Sustain. Energy Rev.* **2007**, *11*, 401–425. [CrossRef]
38. Maeda, K. Photocatalytic water splitting using semiconductor particles: History and recent developments. *J. Photochem. Photobiol. C Photochem. Rev.* **2011**, *12*, 237–268. [CrossRef]
39. Shankhamala, K.; Ciston, J.; Senanayake, S.D.; Arena, D.A.; Fujita, E.; Stacchiola, D.; Barrio, L.; Navarro, R.M.; Fierro, J.L.G.; Rodriguez, J.A. Exploring the Structural and Electronic Properties of Pt/Ceria-Modified TiO_2 and its Photocatalytic Activity for Water Splitting under Visible Light. *J. Phys. Chem. C* **2012**, *116*, 14062–14070.
40. Guisheng, L.; Dieqing, Z.; Jimmy, C.Y. Thermally stable ordered mesoporous CeO_2/TiO_2 visible-light photocatalysts. *Phys. Chem. Chem. Phys.* **2009**, *11*, 3775–3782.
41. Holz, M.C.; Kähler, K.; Tölle, K.; van Veen, A.C.; Muhler, M. Gas-phase oxidation of 2-propanol over Au/TiO_2 catalysts to probe metal–support interactions. *Phys. Status Solidi B* **2013**, *250*, 1094–1106. [CrossRef]
42. Liu, S.Y.; Yang, S.M. Complete oxidation of 2-propanol over gold-based catalysts supported on metal oxides. *Appl. Catal. Gen.* **2008**, *334*, 92–99. [CrossRef]
43. Manriquez, M.E.; López, T.; Gómez, R.; Navarrete, J. Preparation of TiO_2–ZrO_2 mixed oxides with controlled acid–basic properties. *J. Mol. Catal. Chem.* **2004**, *220*, 229–237. [CrossRef]

44. Haffad, D.; Chambellan, A.; Lavalley, J.C. Propan-2-ol transformation on simple metal oxides TiO_2, ZrO_2 and CeO_2. *J. Mol. Catal. A Chem.* **2001**, *168*, 153–164. [CrossRef]
45. Hirakawa, T.; Kamat, P.V. Charge Separation and Catalytic Activity of Ag@TiO_2 Core−Shell Composite Clusters under UV−Irradiation. *J. Am. Chem. Soc.* **2005**, *127*, 3928–3934. [CrossRef] [PubMed]
46. Kowalska, E.; Abe, R.; Ohtani, B. Visible light-induced photocatalytic reaction of gold-modified titanium(IV) oxide particles: Action spectrum analysis. *Chem. Commun.* **2009**, *2*, 241–243. [CrossRef] [PubMed]
47. Sun, B.; Smirniotis, P.G. Interaction of anatase and rutile TiO_2 particles in aqueous photooxidation. *Catal. Today* **2003**, *88*, 49–59. [CrossRef]
48. Ohno, T.; Sarukawa, K.; Tokieda, K.; Matsumura, M. Morphology of a TiO_2 Photocatalyst (Degussa, P-25) Consisting of Anatase and Rutile Crystalline Phases. *J. Catal.* **2001**, *203*, 82–86. [CrossRef]
49. Aramendìa, M.A.; Borau, V.; Colmenares, J.C.; Marinas, A.; Marinas, J.M.; Navìo, J.A.; Urbano, F.J. Modification of the photocatalytic activity of Pd/TiO_2 and Zn/TiO_2 systems through different oxidative and reductive calcination treatments. *Appl. Catal. B: Environ.* **2008**, *80*, 88–97. [CrossRef]
50. Hinojosa-Reyes, M.; Rodríguez-González, V.; Zanella, R. Gold nanoparticles supported on TiO_2–Ni as catalysts for hydrogen purification via water–gas shift reaction. *RSC Adv.* **2013**, *4*, 4308–4316. [CrossRef]
51. Choudhury, B.; Borah, B.; Choudhury, A. Ce–Nd codoping effect on the structural and optical properties of TiO_2 nanoparticles. *Mater. Sci. Eng. B* **2013**, *178*, 239–247. [CrossRef]
52. Contreras-García, M.E.; García-Benjume, M.L.; Macías-Andrés, V.I.; Barajas-Ledesma, E.; Medina-Flores, A.; Espitia-Cabrera, M.I. Synergic effect of the TiO_2-CeO_2 nanoconjugate system on the band-gap for visible light photocatalysis. *Mater. Sci. Eng. B* **2014**, *183*, 78–85. [CrossRef]
53. Martínez-Arias, A.; Gamarra, D.; Hungría, A.B.; Fernández-García, M.; Munuera, G.; Hornés, A.; Bera, P.; Conesa, J.C.; Cámara, A.L. Characterization of Active Sites/Entities and Redox/Catalytic Correlations in Copper-Ceria-Based Catalysts for Preferential Oxidation of CO in H_2-Rich Streams. *Catalysts* **2013**, *3*, 378–400. [CrossRef]
54. Ilieva, L.; Petrova, P.; Pantaleo, G.; Zanella, R.; Liotta, L.F.; Georgiev, V.; Boghosian, S.; Kaszkur, Z.; Sobczak, J.W.; Lisowski, W.; et al. Gold catalysts supported on Y-modified ceria for CO-free hydrogen production via PROX. *Appl. Catal. B Environ.* **2016**, *188*, 154–168. [CrossRef]
55. Mamontov, E.; Egami, T.; Brezny, R.; Koranne, M.; Tyagi, S. Lattice Defects and Oxygen Storage Capacity of Nanocrystalline Ceria and Ceria-Zirconia. *J. Phys. Chem. B* **2000**, *104*, 11110–11116. [CrossRef]
56. Vindigni, F.; Manzoli, M.; Damin, A.; Tabakova, T.; Zecchina, A. Surface and Inner Defects in Au/CeO_2 WGS Catalysts: Relation between Raman Properties, Reactivity and Morphology. *Chem. Eur. J.* **2011**, *17*, 4356–4361. [CrossRef] [PubMed]
57. Kim, Y.I.; Atherton, S.J.; Brigham, E.S.; Mallouk, T.E. Sensitized layered metal oxide semiconductor particles for photochemical hydrogen evolution from non sacrificial electron donors. *J. Phys. Chem.* **1993**, *97*, 11802–11810. [CrossRef]
58. Galindo, F.; Gómez, R.; Aguilar, M. Photodegradation of the herbicide 2,4-dichlorophenoxyacetic acid on nanocrystalline TiO_2–CeO_2 sol–gel catalysts. *J. Mol. Catal. Chem.* **2008**, *281*, 119–125. [CrossRef]
59. Claus, P.; Brückner, A.; Mohr, C.; Hofmeister, H. Supported Gold Nanoparticles from Quantum Dot to Mesoscopic Size Scale: Effect of Electronic and Structural Properties on Catalytic Hydrogenation of Conjugated Functional Groups. *J. Am. Chem. Soc.* **2000**, *122*, 11430–11439. [CrossRef]
60. Porter, J.F.; Li, Y.-G.; Chan, C.K. The effect of calcination on the microstructural characteristics and photoreactivity of Degussa P-25 TiO_2. *J. Mater. Sci.* **1999**, *34*, 1523–1531. [CrossRef]
61. Ohtani, B. Titania Photocatalysis beyond Recombination: A Critical Review. *Catalysts* **2013**, *3*, 942–953. [CrossRef]
62. Watanabe, S.; Ma, X.; Song, C. Characterization of Structural and Surface Properties of Nanocrystalline TiO_2−CeO_2 Mixed Oxides by XRD, XPS, TPR, and TPD. *J. Phys. Chem. C* **2009**, *113*, 14249–14257. [CrossRef]
63. Sun, X.; Liu, H.; Dong, J.; Wei, J.; Zhang, Y. Preparation and Characterization of Ce/N-Codoped TiO_2 Particles for Production of H_2 by Photocatalytic Splitting Water Under Visible Light. *Catal. Lett.* **2010**, *135*, 219–225. [CrossRef]

© 2016 by the authors; licensee MDPI, Basel, Switzerland. This article is an open access article distributed under the terms and conditions of the Creative Commons Attribution (CC-BY) license (http://creativecommons.org/licenses/by/4.0/).